minerals

MDPI

Article

2D and 3D Seismic Survey for Sandstone-Type Uranium Deposit and Its Prediction Patterns, Erlian Basin, China

Qubo Wu [1,2,*], Yanchun Wang [1], Ziying Li [2,*], Baoping Qiao [2], Xiang Yu [3], Weichuan Huang [2], Chengyin Cao [2], Ziwei Li [2], Ziqiang Pan [2] and Yucheng Huang [2]

[1] School of Geophysics and Information Technology, China University of Geosciences, Beijing 100083, China; w123y@163.com
[2] CNNC Key Laboratory of Uranium Resource Exploration and Evaluation Technology, Beijing Research Institute of Uranium Geology, Beijing 100029, China; qiaobaoping@briug.cn (B.Q.); huangweichuan@briug.cn (W.H.); qingping626@126.com (C.C.); liziwei@briug.cn (Z.L.); hedipan@163.com (Z.P.); huangyucheng@briug.cn (Y.H.)
[3] China National Uranium Corporation, China Nuclear Geology, Beijing 100013, China; yuxiang219@126.com
* Correspondence: wdyqthl@163.com (Q.W.); liziying@briug.cn (Z.L.); Tel.: +86-010-6496-3201 (Q.W.)

Abstract: The Erlian basin is one of the most important basins in northern China to host sandstone-type uranium deposits (SUDs), in which Bayanwula, Saihangaobi, and Hadatu are under development, to name a few. Issues such as the metallogenic mechanism and mineralization of these deposits need to be addressed throughout the mining process. Over the past several decades, 2D and 3D seismic reflection surveys have been carried out to study these typical SUDs. The seismic technique has become the most effective geophysical tool of uranium (U) exploration, and it is used to develop our understanding of the stratigraphic configuration, faults, and sandstone contents of target layers in uranium environments. In addition, seismic interpretation could yield useful suggestions regarding the subsequent drilling program in the work area. There are two seismically predictable patterns of SUDs, named "Big depression + fault" and "Large-angle unconformity + fault", which have been established following detailed seismic research in this basin. The characteristics of these faults are as follows: (1) the "'U'-shaped formation" is conducive to the inflow of O-U-bearing groundwater into the target sandstone; (2) the "Big depression of reductive formation" provides plenty of organic matter (containing reducing media and U pre-enrichment) to promote redox reaction mineralization; (3) "Large-angle unconformity" is favorable to the migration of reducing substances, consequently leading to an enhancement in redox U mineralization; (4) "faults with long-term activity" become rising channels for reducing the presence of fluids and gases at depth; and (5) "sandstone and its scrambled seismic facies". The results also offer indirect evidence of a connection between hydrothermal fluids and U mineralization; a hypothesis of "hydrothermal effusion" mineralization is proposed accordingly. In conclusion, seismically produced images of geological structures and sandstone distribution could yield important information for U prospecting and mine planning; it is worth considering seismic technologies in the future exploration of SUDs.

Keywords: Erlian basin; Bayanwula; Saihangaobi; Hadatu; sandstone-type uranium deposit; seismic reflection; seismic response characteristics; prediction pattern

check for updates

Citation: Wu, Q.; Wang, Y.; Li, Z.; Qiao, B.; Yu, X.; Huang, W.; Cao, C.; Li, Z.; Pan, Z.; Huang, Y. 2D and 3D Seismic Survey for Sandstone-Type Uranium Deposit and Its Prediction Patterns, Erlian Basin, China. *Minerals* **2022**, *12*, 559. https://doi.org/10.3390/min12050559

Academic Editor: Michał Malinowski

Received: 18 April 2022
Accepted: 26 April 2022
Published: 29 April 2022

Publisher's Note: MDPI stays neutral with regard to jurisdictional claims in published maps and institutional affiliations.

Copyright: © 2022 by the authors. Licensee MDPI, Basel, Switzerland. This article is an open access article distributed under the terms and conditions of the Creative Commons Attribution (CC BY) license (https://creativecommons.org/licenses/by/4.0/).

1. Introduction

Since the China National Nuclear Corporation (CNNC) began exploring sandstone-type uranium deposits in the 1990s [1,2], a number of SUDs have been discovered in northern China, in the Mesozoic strata [3]. SUDs have become one of the fastest growing types of uranium storage in China in recent years, accounting for approximately 40% of the total reserves [4,5]. The Honghaigou, Mengqiguer, and Langka deposits were successively identified in the Yili basin, NE China [6–8], whereas the Dongsheng and Daying deposits were identified in the Ordos basin, north China [9–11] and the Qianjiadian deposits in the

Songliao basin, NE China [12,13]; many other uranium ore fields have been explored in the last ten years. These also include the Bayanwula, Saihangaobi, Qiharugetu, and Hadatu deposits in the Erlian basin [14–16]. The uranium deposits in the Erlian basin are the most dispersed, have the most complex mineralization conditions, and are the largest in number [17]. In view of this, much geological research work has been carried out in the Erlian basin, including studies of sedimentology [18,19], tectonics [20,21], mineralogy [22,23], and geochemical exploration [24–26]. It has been found that the evolutionary conditions of mineralization are closely related to deposit formation (FM), geological structure, faults, the sand body of the target layer, sedimentary facies, and other factors, most of which are not easy to observe from the surface. Surface-based geological surveys cannot look inside the Earth, and drilling projects cost too much [27]. Consequently, researchers have had to utilize geophysical prospecting to reveal the U mineralization environment and its influencing factors. Some developments have been made, for example: (1) gravity data have been used to roughly divide large-scale structures and mineralization-favoring regions; however, given the low accuracy of these gravity models, the depth formations are insufficient [28,29]. (2) High-precision magnetic testing of the Bayanwula SUD in the Erlian basin showed that the distribution of the redox zone can be inferred from magnetic anomalies, but this indicator may be unusable when complex geological conditions are present, such as large overburden areas, and so its effectiveness requires further testing [30,31]. (3) Good-quality information pertaining to the detection of shallow volcanic rocks and large sets of sand bodies (over 60 m thickness) can be obtained using the electromagnetic method in uranium deposit basins, but this approach struggles to accurately identify the interfaces of layers and thin sand bodies [32,33]. (4) Electromagnetic sounding performed well in paleochannel SUD surveys in South Australia and North America, and the characteristic logging responses of the alteration zone were studied to locate the redox boundaries in the work area [34]; nevertheless, the depth of the target layer was too shallow. (5) Seismic exploration technologies have played an important role in determining the stratification, faults, geological structure, lithology (especially in sand bodies), sedimentary facies, and paleochannels in the Erlian basin [35–39], and this method has also been applied to derive detailed images of ore-controlling faults, alternated zones, and unconformities in another kind of deposit, namely, unconformity-related uranium deposits in the Athabasca basin in Canada [40–43]. (6) Three-dimensional seismic attributes offer effective signals of the sedimentary characteristics of SUD formations [44]. Accordingly, seismic techniques are now accepted as the most effective means to visualize the underground uranium mineralization environment besides expensive drilling, with better accuracy than other geophysical methods can achieve.

However, seismic exploration methods have not been extensively tested and applied in the Erlian basin, even though this is a large resource area, and the pattern of prediction for U mineralization is still unclear. Initial reflection reconnaissance tests have deduced the geological structure and velocity variations of sandstone in a specific area using seismic attributes, but their achievements were limited when applied to shallow images [45]. A successful test of seismic reflection mapping was carried out by the Beijing Research Institute of Uranium Geology (BRIUG) from 2010 to 2013, based on the BIG BASE plan of CNNC. Since then, other seismic projects have been undertaken, such as the HEXIN project in 2015 (which is undertaking unique 3D seismic study work at the CNNC) and the Long Can phase II project, which began in 2018, also at the CNNC. Many achievements have been made in these studies [46,47], including the provision of detailed maps of the structures and faults controlling the ore deposits, clarification of the subsurface stratification that determines mineralization, and the development of more effective technologies for the acquisition, processing, and interpretation of SUD reflection data. However, there is still a lack of systematic geophysical results (especially seismic ones) and geophysical prediction patterns for the main SUDs in the Erlian basin derived from seismic data, which means that uranium engineers are at a loss when they receive seismic data to be interpreted.

The purpose of this work is to fully extract the features of the most favorable U mineralization environment from 2D and 3D seismic data that have been accumulated over a few years for the Erlian basin. We have aimed to construct a prediction pattern of U mineralization in order to improve the applicability of seismic exploration technology to SUDs in the future. This study is mainly split into three parts: the introduction of methods of seismic data acquisition for the processing and interpretation of SUDs; the seismic response characteristics of typical SUDs; and two common prediction patterns seen in U-containing environments.

2. Geologic Setting

2.1. Basin and Formation

The Erlian basin (or Erenhot basin)—containing five NE-trending sub-basins, named Chuanjing, Wulanchabu, Manite, Wunite, and Tenggeer, and a Sunite uplift (Figure 1)—is located on the suture belt between the Siberian craton and the North China craton in NE China [48,49]. Its basement is primarily composed of mediocre Paleozoic metamorphic and Jurassic volcanic rocks [50]. It comprises mainly Cretaceous, Palaeogene, Neogene, and Quaternary strata, containing lacustrine and fluvial deposits. The Cretaceous Arshan Group (K_1a) and Tengger Group (K_1t) are both oil-bearing layers, whereas the Saihan Group (K_1s) is coal-bearing and is the major uranium-bearing formation in this basin. The Erlian Group (K_2e) is the secondary target layer, with Palaeogene, Neogene, and Quaternary sediments as the main alluvial deposits. Previous comprehensive studies have shown that the Erlian basin is typical of the rift-type one. The early syn-rift deposits in K_1a are irregularly underlain with K_1t, which is irregularly covered by K_1s and K_2e, and the overlying strata are the post-rift filling sediments [51].

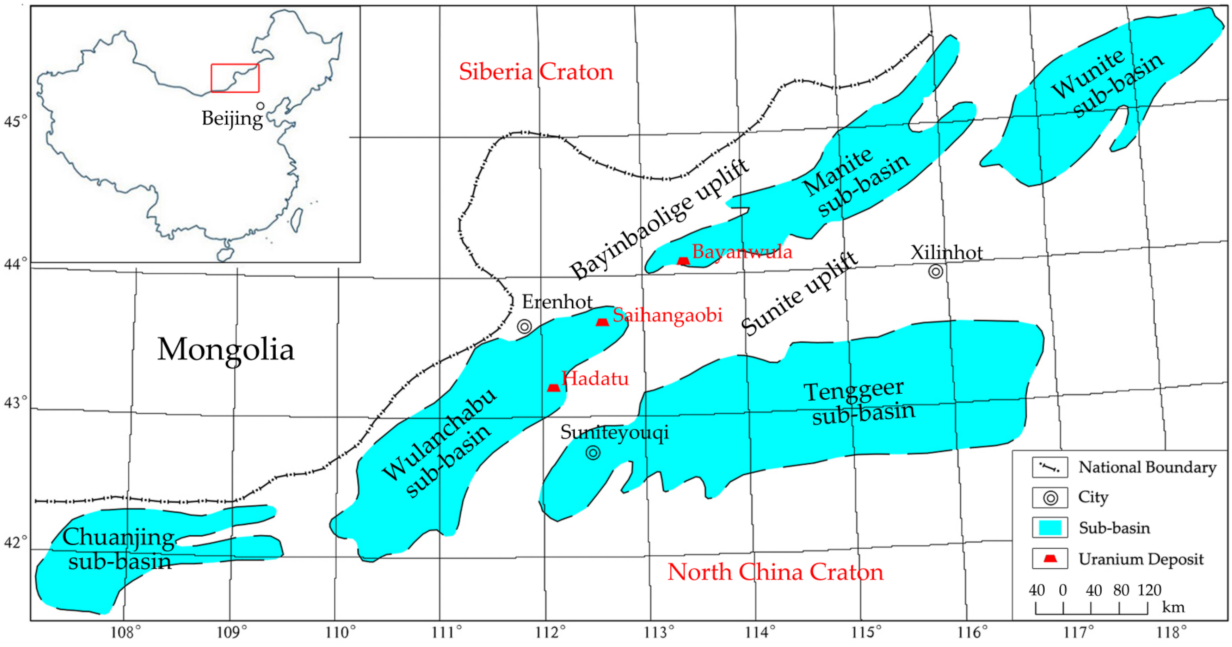


Figure 1. Tectonic units of Erlian basin and the distribution of SUDs (modified from Qiu et al. [49]).

2.2. Sandstone-Type Uranium Deposit

A number of different media and large SUDs have been identified, including the Bayanwula deposits in the Manite depression, and the Saihangaobi, Hadatu, and Qiaoergu deposits in the Wulanchabu depression. Most of the deposits discovered so far are mainly of sandstone-hosted tabular or roll-front types [52], which facilitate the most economically viable uranium mines owing to their amenability to the low-cost in situ leaching extraction of U. It is broadly believed that SUD mineralization in the Erlian basin depends on reduction with sulfides and organic matter [53], and this is attributed to the presence of hydrocarbon

fluids derived from recent electron probe and geochemistry studies [49], but there is no other proof of this.

2.3. Rock Physical Parameters

(1) Density: The average density of Quaternary FM is 1.45 g/cm^3, whereas it is 1.78 g/cm^3 for Neogene and 1.67 g/cm^3 for Palaeogene, 2.03 g/cm^3 for Cretaceous, 2.55 g/cm^3 for Jurassic, and over 2.66 g/cm^3 for Paleozoic (shown in the Table 1). There are obvious density differences between layers. There are also distinct density differences between different types of rocks—the density increases from 1.8 g/cm^3 to 2.3 g/cm^3 when the lithology shifts, step by step, from mudstone to fine sandstone, mid-fine-grained sandstone, sandstone, conglomeratic sandstone, and conglomerates. There is a density increment from acidic rocks to neutral and ultrabasic rocks, whereby the density of Yanshanian acid rocks is about 2.55 g/cm^3, whereas it is 2.68 g/cm^3 in Caledonian period rocks and 2.66 g/cm^3 in Archeozoic rocks, and the densities of neutral and superbase rocks are generally above 2.70 g/cm^3.

Table 1. The physical parameters of formations and rocks in Erlian basin (modified from Wu et al. [54]).

Stratum Symbol		Lithology	Density (g/cm^3)	Acoustic Velocity (m/s)
Q		Gravel, clay	Avg 1.45	800–1250
N	N_2	Pebbled sandstone	Avg 1.51	1100–1500
	N_1		Avg 2.05	
E	E_3	Mudstone, siltstone	Avg 1.84	1100–2500
	E_2		Avg 1.47	
	E_1		Avg 1.46	
K	K_2	Mudstone	1.8–2.0	1380–1780
		Siltstone	1.9–2.1	2050–2380
		Fine sandstone	1.9–2.2	2050–2630
		Sandstone	2.0–2.2	2050–2630
		Sandy conglomerate	2.1–2.3	2940–3700
	K_1	Mudstone	1.8–2.0	1500–1660
		Siltstone	1.9–2.1	1610–1750
		Sandstone	1.9–2.1	2560–4340
		Sandy conglomerate	1.9–2.3	2850–4160
J	J_3	Limestone, volcanic	Avg 2.53	2630–3220
	J_2		Avg 2.58	
	J_1		Avg 2.52	
P	P_2	Slate, limestone, volcanic	Avg 2.67	<3220
	P_1		Avg 2.66	
Acid rocks			2.55–2.59	3030–6250
Middle acid rock			2.63–2.66	
Basic extrusive rocks			2.69–2.80	
Basic intrusive rock			2.81–2.83	
Ultrabasic rock			2.63–3.31	

(2) Acoustic properties: The acoustic velocity in the Quaternary and Tertiary strata ranges from 800 to 1250 m/s, whereas it is 1380 to 3700 m/s in Upper Cretaceous FM,

1500–1340 m/s in Lower Cretaceous, 2630–3220 m/s in Jurassic, below 3220 m/s in Paleozoic strata, and below 6250 m/s in volcanic rocks (shown in the Table 1). Mudstone and fine sandstone have low acoustic velocities of about 1500 m/s, whereas the velocity of coarse sandstone and conglomeratic sandstone is over 2300 m/s, making it the basis for seismic exploration in the study area.

3. Seismic Reflection

3.1. Data Acquisition

Four seismic exploration phases have been undertaken in the Erlian basin since 2004. The first seismic test was conducted by the Airborne Survey and Remote Sensing Center of the CNNC from 2004 to 2006 in the Bayanwula deposits. At that time, simple instruments and a small amount of explosive were utilized, along with 6-fold acquisition; using this equipment, the deep geological structure could hardly be seen. With the subsequent seismic programs BIG BASE and LONG CAN, both carried out by the Beijing Research Institute of Uranium Geology of the CNNC (BRIUG) from the year 2009 to 2019 at some key sites in the basin, advancements in both hardware and software technologies enabled rapid improvements in the effectiveness of exploration due to the fold increase (24~60) that was introduced when using big vibrators and noise attenuation with combined receiving. The HEXIN 3D seismic exploration project is the only 3D project to be undertaken in the CNNC to date, and it was successfully conducted by BRIUG, yielding a series of high-resolution images of the subsurface properties of the work area. The acquisition parameters of these seismic projects are summarized in Table 2 [55]. The most effective modification of shallow seismic imaging for SUDs involved using broadband frequency vibrators (3–120 Hz), high-fold acquisition (about 60), and low-frequency geophones (5~10 Hz), because broadband frequency seismic information can be used to improve the bandwidth of the initial inversion model, which improves the inversion accuracy of thin beds of sandstone. Meanwhile, we can utilize a smaller bin size (5~10 m) to improve shallow imaging, and we also employed a lighter vibrator to obtain the seismic data of shallow SUDs (instead of the heavier 28,000 kg one), which enabled a considerable cost reduction.

Table 2. Acquisition parameters of 2D and 3D seismic survey in four stages.

Items	TEST(2D)	BIG BASE(2D)	LONG CAN(2D)	HEXIN(3D)
Recording instrument	Summit II, NZXP	NZXP, ARIES, IMAGE	Sercel 428XL	Sercel 428XL
Record length(s)	1	4	4	4
Source and excited pattern	200 g explosive	1.5–2 kg explosive, KZ28 28,000 kg vibrator (10–80 Hz, 2–4 sweeps, 12 s length)	EV56 28,000 kg vibrator (3–110 Hz, 1–2 sweeps, 10 s length)	BV-620LF 28,000 kg vibrator (3–120 Hz, 1–2 sweeps, 10 s length)
Source interval(m)	40	20–40	20	20
Geophones group interval (m)	20	10	10	10
Geophones per group	1	1–4 at one receiving point	4–10 at one receiving point	4 at one receiving point
Natural frequency of Geophone (Hz)	60	10–40	10	5
Number of recording channels	24	144	240	2048
Folds	6	24	60	120

3.2. Data Processing

In general, the raw data obtained from these surveys have different features, but a common trait is the quality of the shallow noise, especially the coherence noise and the surface waves. Furthermore, strong reflective energy can be seen at the interfaces between K_1s and K_1t, K_1a and the basement, etc. The key procedures for processing SUD seismic data can be summed up as follows: (1) different types of noise are often found in the shallow parts of an SUD's seismic record, so the combination of denoising methods with frequency-divided denoising, adaptive surface wave attenuation, and coherent noise suppression could achieve good results; (2) the accuracy of velocity analysis is very important during

the shallow imaging of SUDs, and residual static corrections (usually three iterations) would greatly improve its resolution; (3) expanding the frequency band of post-stack data as far as possible improves the inversion, which is a significant factor when identifying thin beds that may contain U mineralization. In order to achieve this last goal, combined deconvolution and inverse Q filtering methods are commonly applied.

An effective workflow facilitating the enhanced processing of 3D seismic data is shown in Figure 2. As for 2D seismic data, post-stack time migration is used.

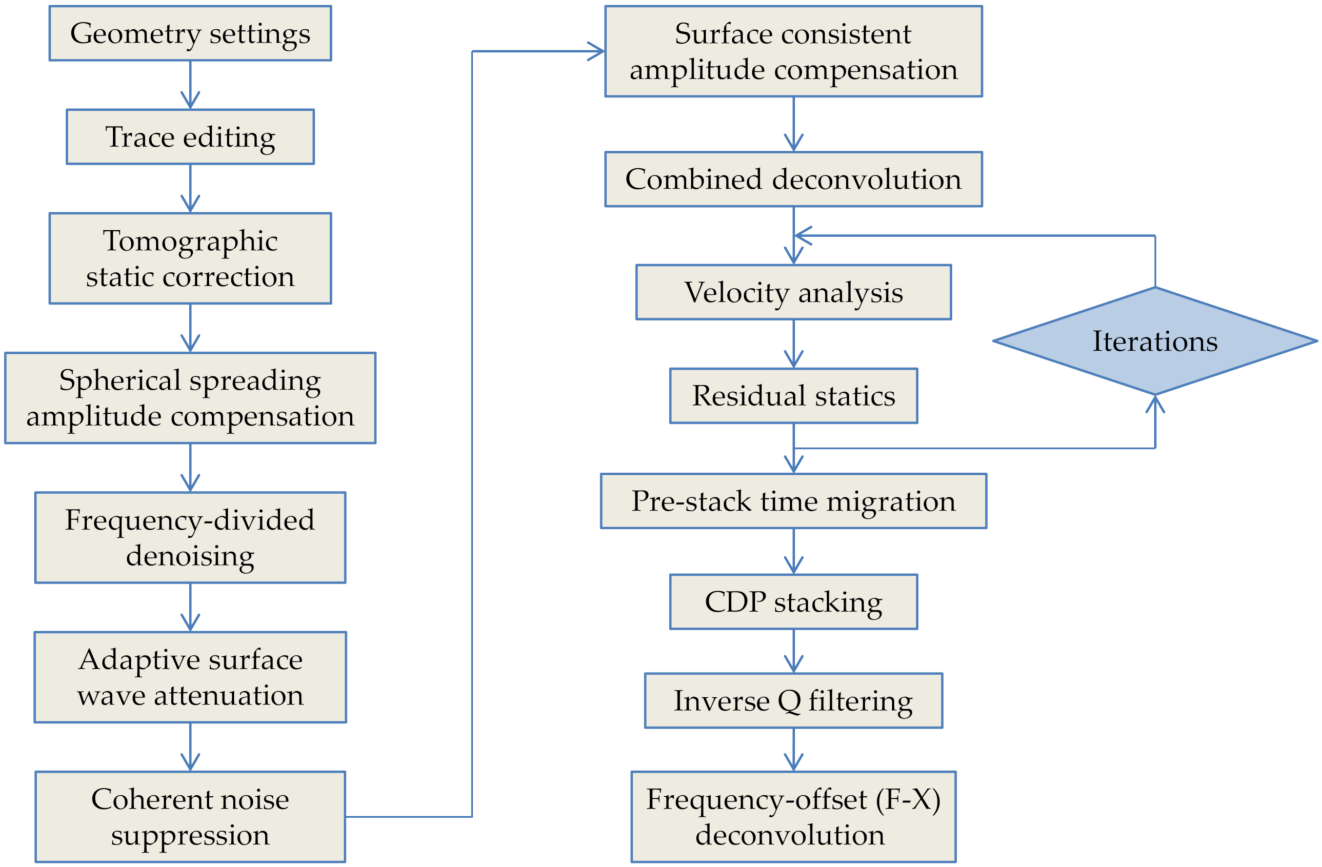


Figure 2. Processing workflow for 3D seismic data of a sandstone-type uranium deposit (modified from Wu et al. [56]).

3.3. Interpretation and Inversion

The study of stratigraphy and structural morphology is the fundamental aim of seismic data interpretation and inversion in SUDs' metallogenic environments. The target formation range reaches from K_2e to K_1s^1 in the Erlian basin (shown in Figure 3).

This work first focuses on synthetic seismic correlation. The typical phase is shown in Figure 3, where the purple vertical lines represent the drilling track, and the purple horizontal lines represent the bottoms of geological horizons; the impedances are calculated from the measured velocity and density. Secondly, we perform horizon interpretation based on synthetic seismic correlation, which is central to determining whether target deposits are present; meanwhile, fault interpretation is executed primarily using post-stack data, the seismic coherence attribute, and the instantaneous phase attribute. This is also very important, because these faults may be ancient channels by which reducing agents rose to sufficient depth to promote the redox reaction for U mineralization. Finally, we know that the thickness of uranium-bearing sandstone varies from several meters to dozens of meters, so determining the sandstone distribution is key in SUD seismic inversion, and particularly to improving the accuracy of inversion. In this work, the post-stack impedance inversion and pre-stack elastic inversion methods were applied to interpret sand distribution, and

the resistivity logging inversion was used to improve the resolution of sand prediction based on the lateral seismic constraint. The previous seismic inversion methods could not produce favorable results because of the lack of high-quality acoustic data in shallow target layers, so here, the resistivity and density data are integrated with the acoustic data to produce quasi-acoustic data, which yield good lithology recognition accuracy. Figure 4 shows that the raw acoustic wave curve (blue) and the pseudo-acoustic wave curve (red) overlap in most layers, but in the 510~530 m section, the raw acoustic wave curve does not exactly match with mudstone and siltstone, whereas the pseudo-acoustic wave curve works very effectively. Acoustic data are usually not available because of the inadequate logging of shallow SUDs measurements, and so pseudo-acoustic data may enable the completion of effective inversion.

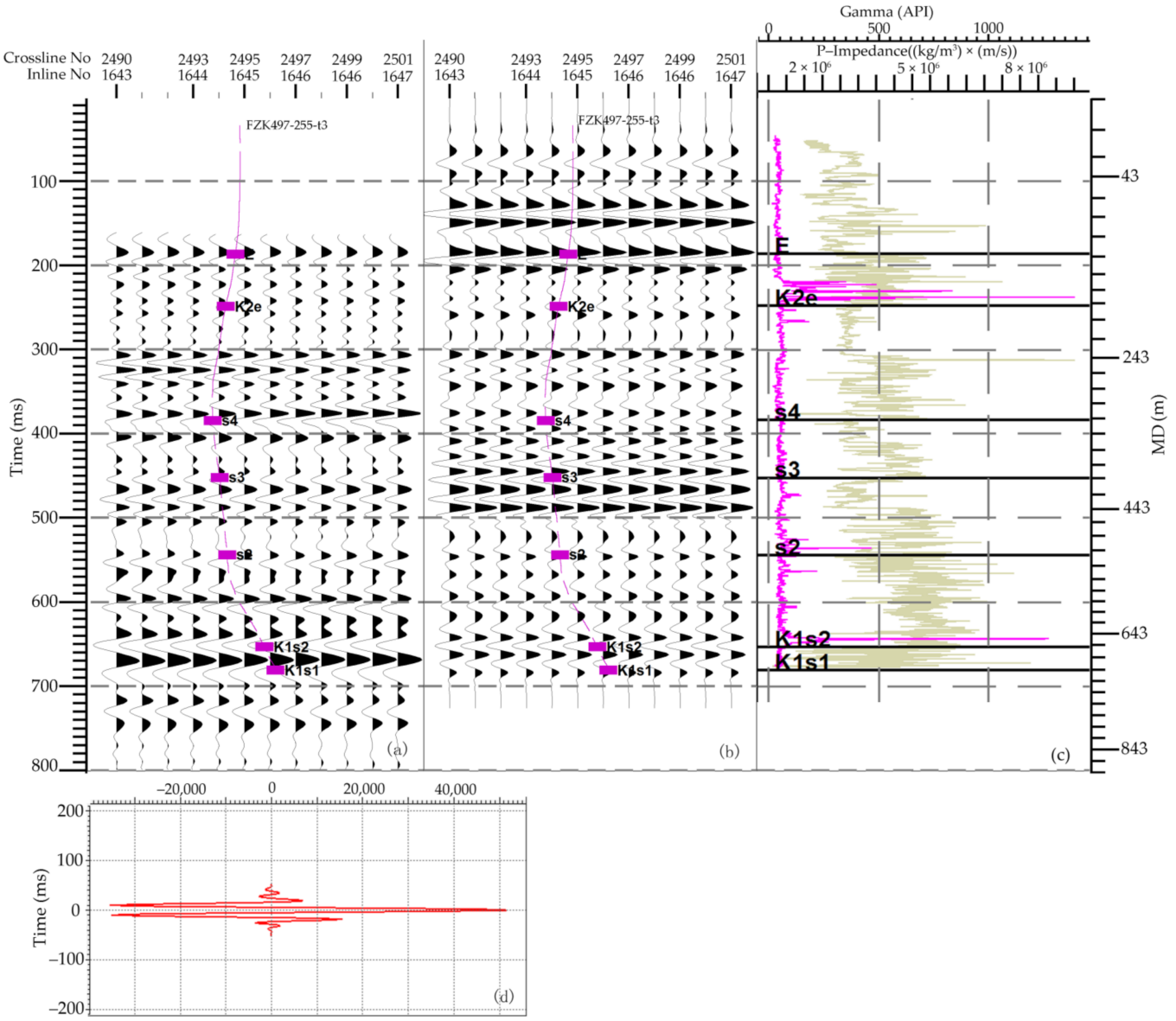


Figure 3. Synthetic seismic calibration of the typical borehole data from the 3D seismic study area. (**a**) the seismic data; (**b**) synthetic model calculated by the convolution of the reflection coefficient and the wavelet; (**c**) the gamma and impedance loggings of the typical well; (**d**) the wavelet extracted from well and seismic data.

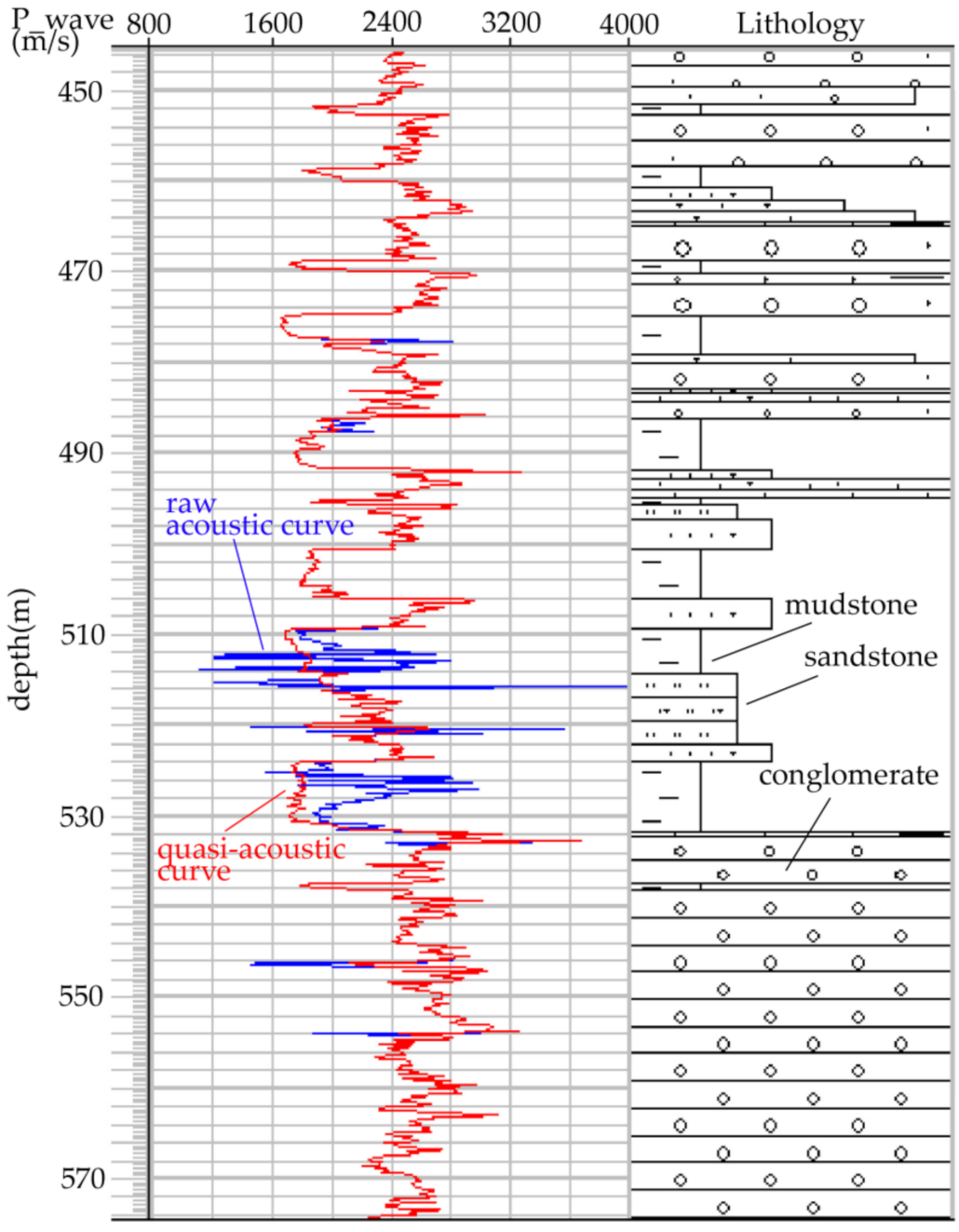


Figure 4. The comparison of the raw acoustic curve and the quasi-acoustic curve for a typical borehole in the 3D seismic study area.

4. Results and Discussion

Our focus has been on obtaining direct or indirect indications of U mineralization from the seismic imaging of typical deposits over the past decade. Several 2D profiles have been completed covering the well-known Bayanwula and Saihangaobi deposits, as well as a 3D seismic network located in the south of the recently discovered Hadatu deposit, which exhibits the highest grade of sandstone uranium mineralization in the Erlian basin. The deployment of all the seismic survey lines is shown in Figure 5. We also know that these three deposits are all located in low-gravitational anomaly or zero-transition zones, which often indicate the bottom or slope of a depression.

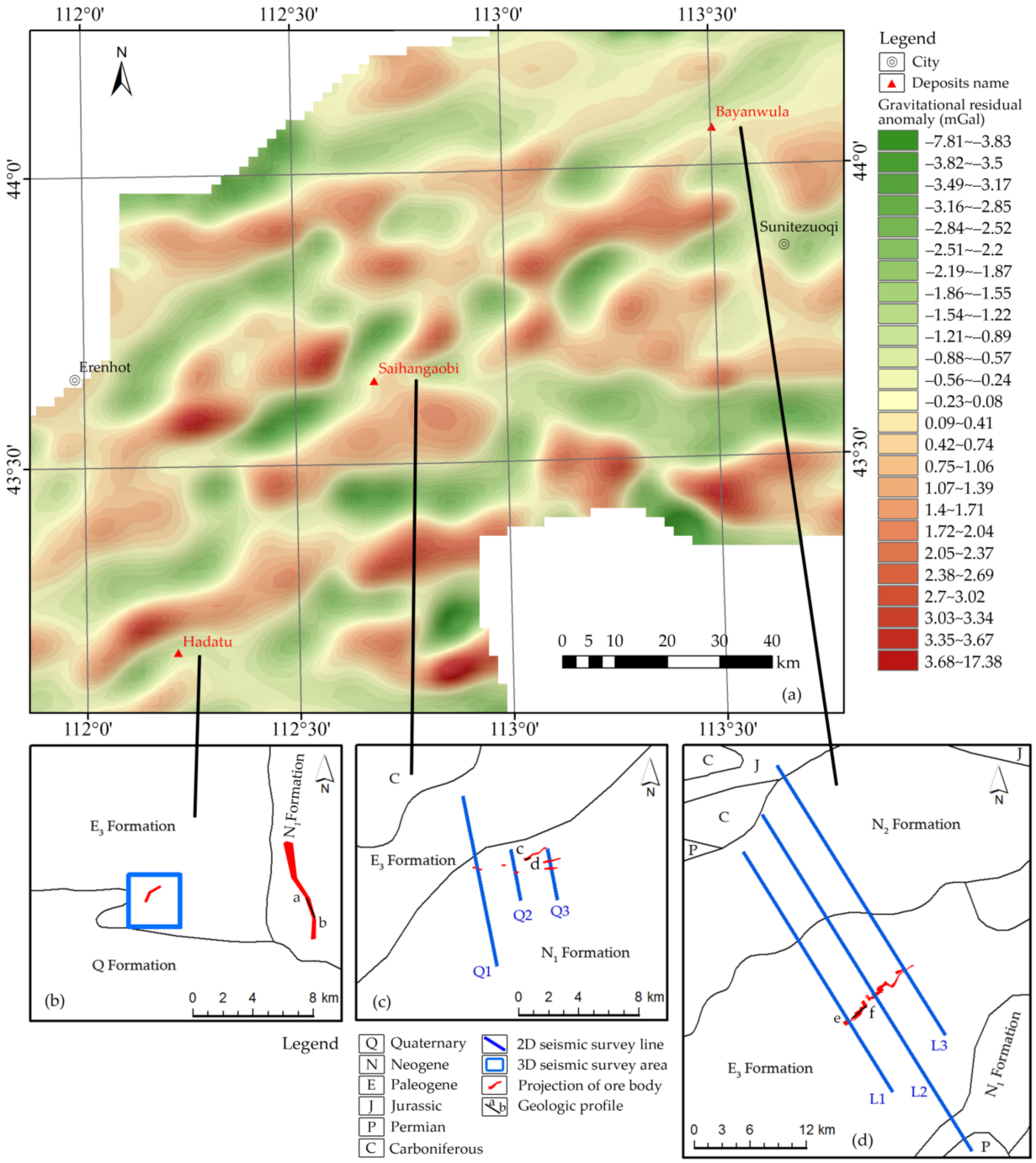


Figure 5. (**a**) Map of gravitational residual anomalies and the deposits' positions in the study area. (**b**) The area of 3D seismic surveys performed in the Hadatu deposit. (**c**) The lines of the 2D seismic survey performed on the Saihangaobi deposit, and (**d**) the lines of the 2D seismic survey performed on the Bayanwula deposit.

4.1. Bayanwula SUD

4.1.1. Background Geology

Bayanwula SUD is located in the west of the Manite sub-basin, within the NE-trending low–medium-gravity field. The Bayanwula paleochannel SUD has similar features to the Wyoming deposit [57], identifying it as a roll-front type deposit; its mineralization is hosted in coarse-grained sandstone, with braided fluvial facies in the upper part of the K_1s FM. The top of the target layer, about 100–250 m deep, is red impermeable mudstone, and the

bottom layer is grey mudstone and Cretaceous coal seam. Previous geological explorations have shown that the oxidation began at the edges (NW and SE) and spread towards the center, which resulted in an ancient NE-trending oxidation belt determining the occurrence of mineralization (Figure 6) [58].

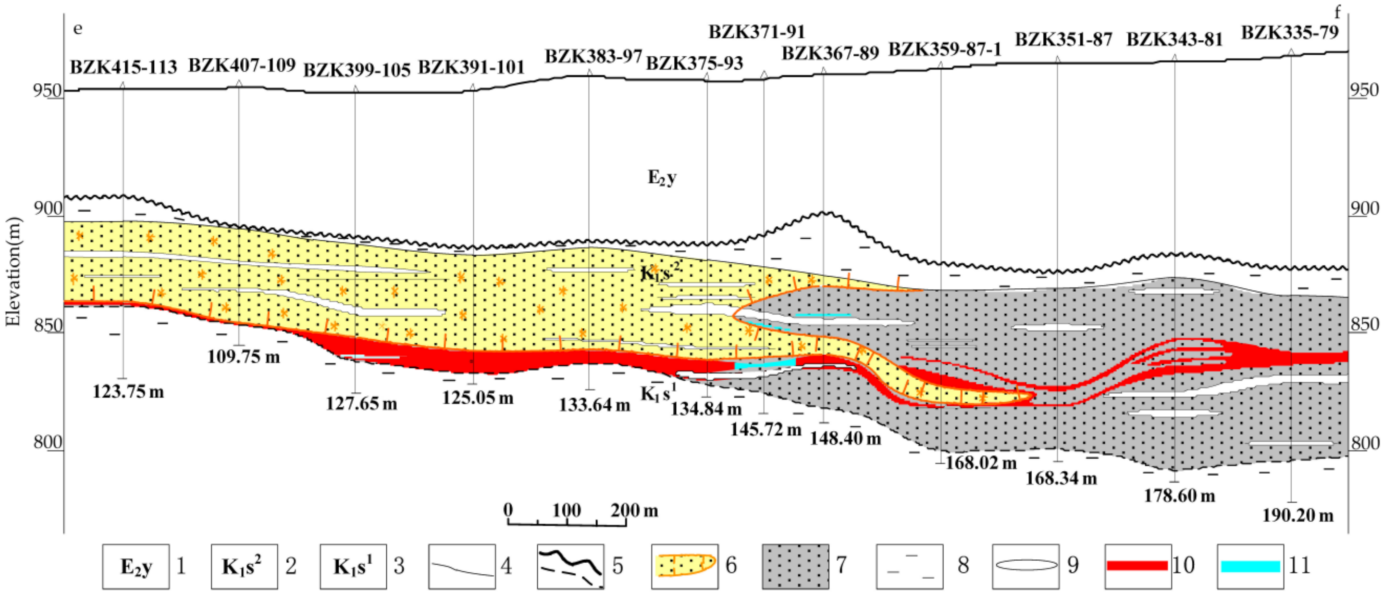


Figure 6. Geological profile of e–f in the Bayanwula uranium deposit. 1—Yierdingmanha group. 2—Upper part of Saihan group. 3—Bottom part of Saihan group. 4—Lithologic boundary. 5— Angle or parallel unconformity boundary. 6—Yellow oxidized sands. 7—Gray reducing sands. 8—Impermeable mudstone. 9—Local impermeable layers. 10—Uranium ore bodies. 11—Uranium mineralization.

4.1.2. Seismic Exploration Result and Its Relationship with Mineralization Environment

The acquisition parameters of the 2D seismic data are shown in Table 1, depicting the TEST stage. First of all, seismic exploration technology is applied to assess the SUD environment, such as the formation configuration, and the presence faults and sand bodies in the target K_1s FM, as well as to potentially explore the seismic response of the U-containing layer.

The interpreted seismic sections along the lines L1, L2, and L3 are shown in Figure 7. The green line represents the bottom of the target layer, the depth of which became increasingly shallow from north to south, but the formation was totally eroded at the northern edge and in the middle of the section because of strong tectonic compression in the vicinity. This also created some faults, mainly normal faults. Industrial uranium mineralization occurred in the middle of the profile, at about 150 m deep.

In Figure 7, the K_1s FM takes on a "U" shape, and the most favorable mineralization sites are located in the two sides of the sloping "U"-shaped belt, with seismic facies of weak–medium amplitude, low–medium frequency, and low continuity, and there are also oil-bearing and coal-containing formations (reducing deposits) below the target "U" formation. As such, the most favorable mining area appears as a "big depression" from top to bottom. Additionally, there are steeply dipping faults and fractures on either side of the "big depression", characterized by reflective breaks; some faults have developed in the reducing formation and extend into the "U"-shaped formation.

The SUD in this area is a typical roll-front oxidized-type uranium deposit [22]. This kind of mineralization process can be briefly described as follows.

Ancient ground water (i.e., oxygen-U^{6+}-bearing fluids) emerged into the provenance (i.e., uplift) area through the sand bodies of the target layer, causing yellow oxidation and alteration. Then, a redox reaction was triggered when the oxidizing fluids described above

met the reducing materials already present in the sand body, resulting in the deposition of U^{4+} and the precipitation of mineralization [53].

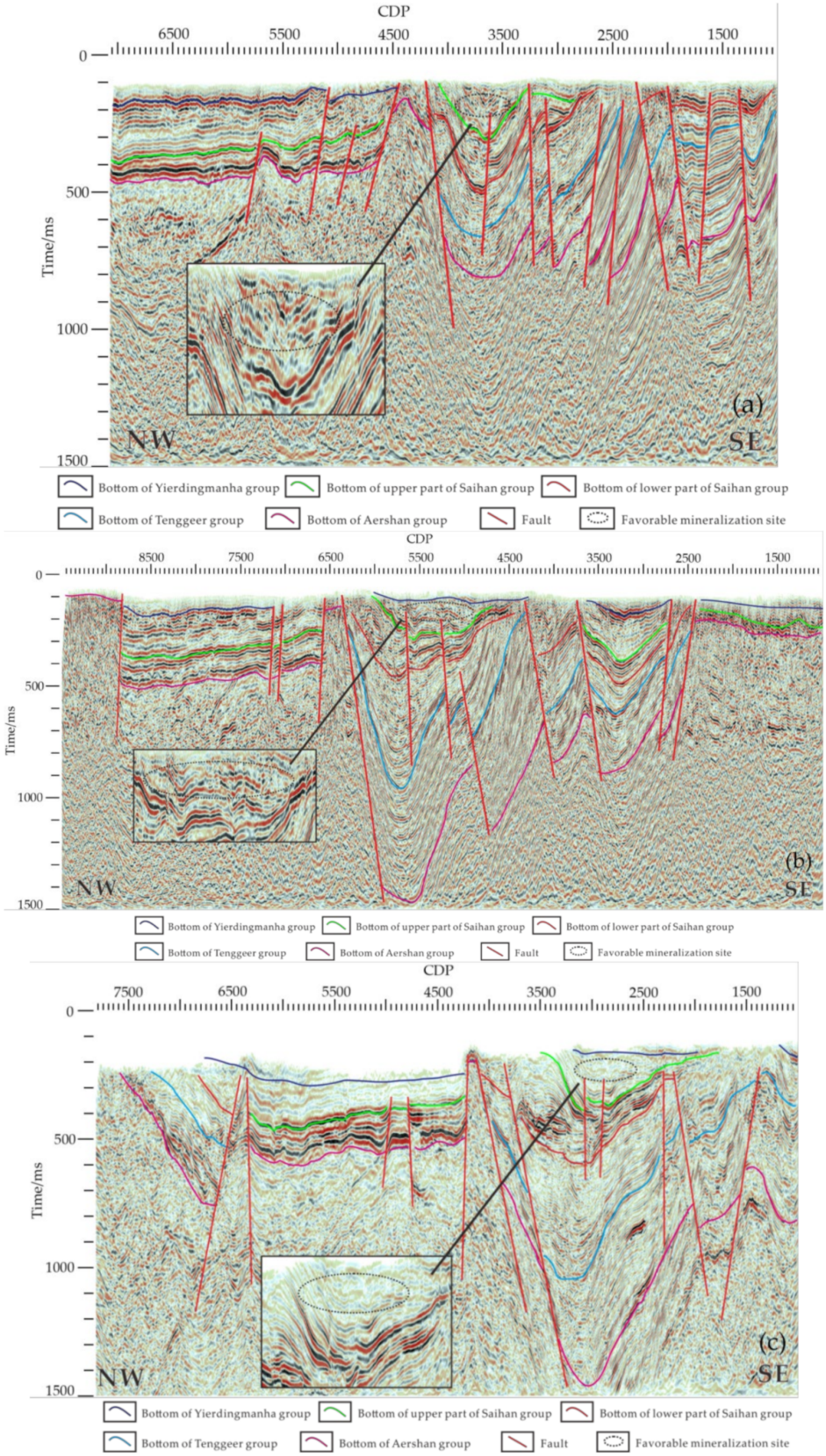


Figure 7. The seismic survey results for the Bayanwula uranium deposits: L1 (**a**), L2 (**b**), L3 (**c**).

The environments most favorable to uranium mineralization could show characteristic seismic responses in the deposits for a variety of reasons. Firstly, the two-winged slopes of the "U"-shaped layer are a naturally favorable zone, and they facilitate lateral oxidation, which is the basis of uranium mineralization; meanwhile, the faults on either side of the "U" formation are the products of structurally inverted uplift, which could improve the hydrological replenishment–runoff–discharge conditions that are of benefit to oxidation and reduction reactions. U mineralization may occur as a result of these reactions. Secondly, the presence of a "big depression" implies the large, deposited thickness of reducing formations, containing sufficient reduction materials; furthermore, the faults extending from the reducing deposits into the target sand bodies could provide channels for the raising of deeply buried reductive mediums, such as gas and fluids. These materials play an important role in the progression of the redox reaction in sand bodies, meaning U mineralization may occur. Finally, in the Bayanwula deposit, the U-bearing sandstones are all derived from poorly sorted sand bodies from the braided river, which is why there are discontinuous seismic faces spread about the mineralization site.

4.2. Saihangaobi SUD

4.2.1. Background Geology

The Saihangaobi SUD is located approximately 50 km southwest of the Bayanwula deposits. It is a paleo-valley-type uranium deposit, featuring significant differences in terms of the phreatic oxidation from roll-front oxidizing deposits. Phreatic oxidation contributes to the presence of tabular ore bodies (Figure 8) similar to those of the Russian Trans-Ural [59] and Colorado [60]; the depth of this type of oxidation varies according to the rock's permeability and the presence of fissures but is generally dozens of meters. The U mineralization containing carbon matter is also hosted within the glutenite braided fluvial deposits in the upper section of K_1s FM, and the top and bottom formations of the target sand layers are dominated by mudstone.

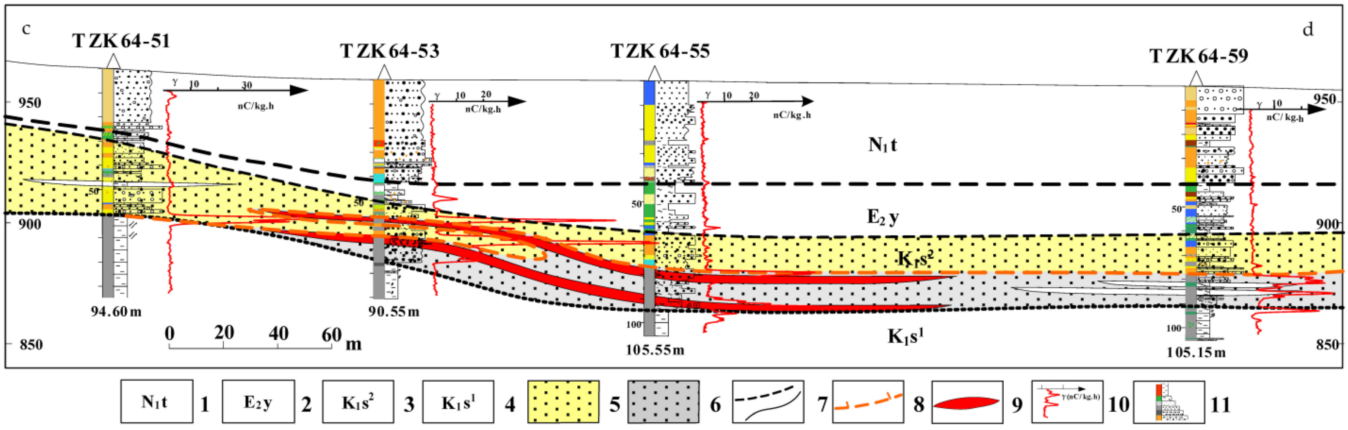


Figure 8. Geological profile of c–d in Saihangaobi uranium deposits. 1—Tongguer group. 2—Yierdingmanha group. 3—Upper part of Saihan group. 4—Bottom part of Saihan group. 5—Yellow oxidized sands. 6—Gray reducing sands. 7—Angle of the parallel unconformity boundary. 8—The oxidation front line. 9—Uranium ore bodies. 10—Gamma logging. 11—Rock particle size histogram and color column.

4.2.2. Two-Dimensional Seismic Survey Results and Their Relationship with Mineralization Environment

The parameters employed when collecting the 2D seismic data are shown in Table 2 (BIG BASE stage). The purpose of the seismic exploration survey of these deposits is the same as in Bayanwula.

A detailed interpretation of the line comprising Q1, Q2, and Q3, superposed on post-stack migration, is given in Figure 9. The bottom interface of the target layer is marked by

a green line, which means there is no target formation in the southern profile, and it is only present in a very thin layer in the north. Furthermore, the ore bodies are at about 100 m deep in the middle of the profile. The northern formations were almost entirely wiped out by the increasing regional uplift, and while the southern deposits were saved, they are dipping steeply downwards as a result of tectonic movement, and this has contributed to the development of some normal faults, marked by red lines.

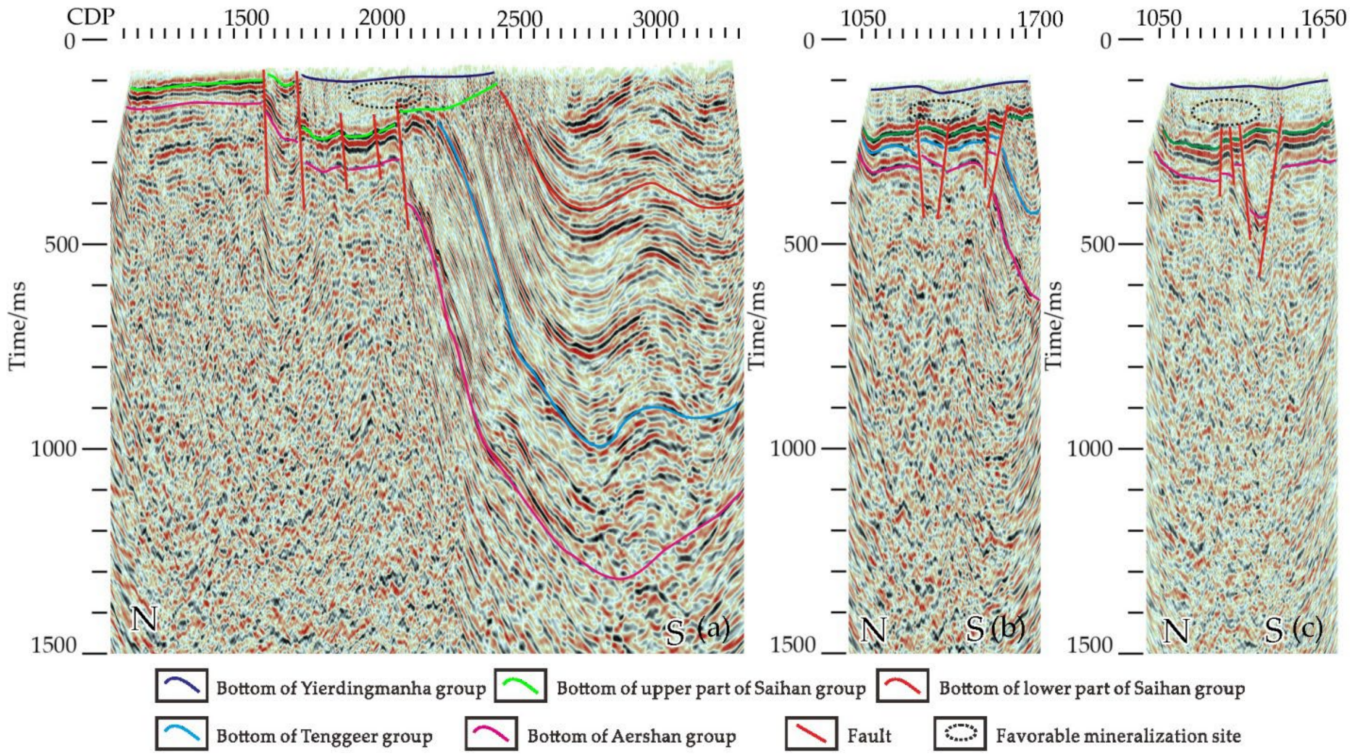


Figure 9. The seismic survey results on Saihangaobi uranium deposits; Q1 (**a**), Q2 (**b**), Q3 (**c**).

The target formation (above the green line) resembles a "U" shape filled with fluviatile deposits. The U mineralization is located on the bottom and the slopes of the "U"; under the target layer, very thick reducing formations have developed that form a "big depression", generally exceeding 1000 m at the deepest point. In the southern section, the reducing formation contacts the overturned "U" formation at a large angle (about 25°). The seismic phase of the mineralization-favoring site shows weak–medium amplitudes, low–medium frequency, low continuity, and a wavelike reflection configuration.

The cause of these seismic response characteristics in the mineralization environment is primarily the same as in the Bayanwula deposit. Uplift has developed on both sides of the "U" formation, the two slope zones of which offer favorable conditions for the lateral oxidation of O-U-bearing fluids. The thick reduction formations of the "big depression" could supply enough reducing medium and pre-enriched uranium, and these materials could rise into the target layers through faults, such that they may be able to enhance the U enrichment of the target sandstone and the reducing capacity of the sand bodies; this reduction ability could promote mineralization. The biggest difference from the Bayanwula deposit is the strengthened reducing capacity; the reductive materials in the "big depression" could easily migrate along interlayer channels into the target sand bodies because of the large-angle non-conformity between the reducing formation and the K_1s FM it covers.

4.3. Hadatu SUD

4.3.1. Background Geology

The recently discovered Hadatu deposit is located in the north-central region of the Wulanchabu sub-basin, roughly 40 km southwest of the Saihangaobi deposits. The U mineralization, with an average grade of 0.1008% [24], is mainly hosted in the gray pebbly sandstone of the K_1s formation and has a tabular ore characteristic (Figure 10). The genesis of this high-grade uranium deposit has not been thoroughly addressed, although some geochemistry and mineralogy studies have been performed. The Hadatu deposits are divided into two districts: one major deposit in the north and an extended deposit in the southern area [19,61].

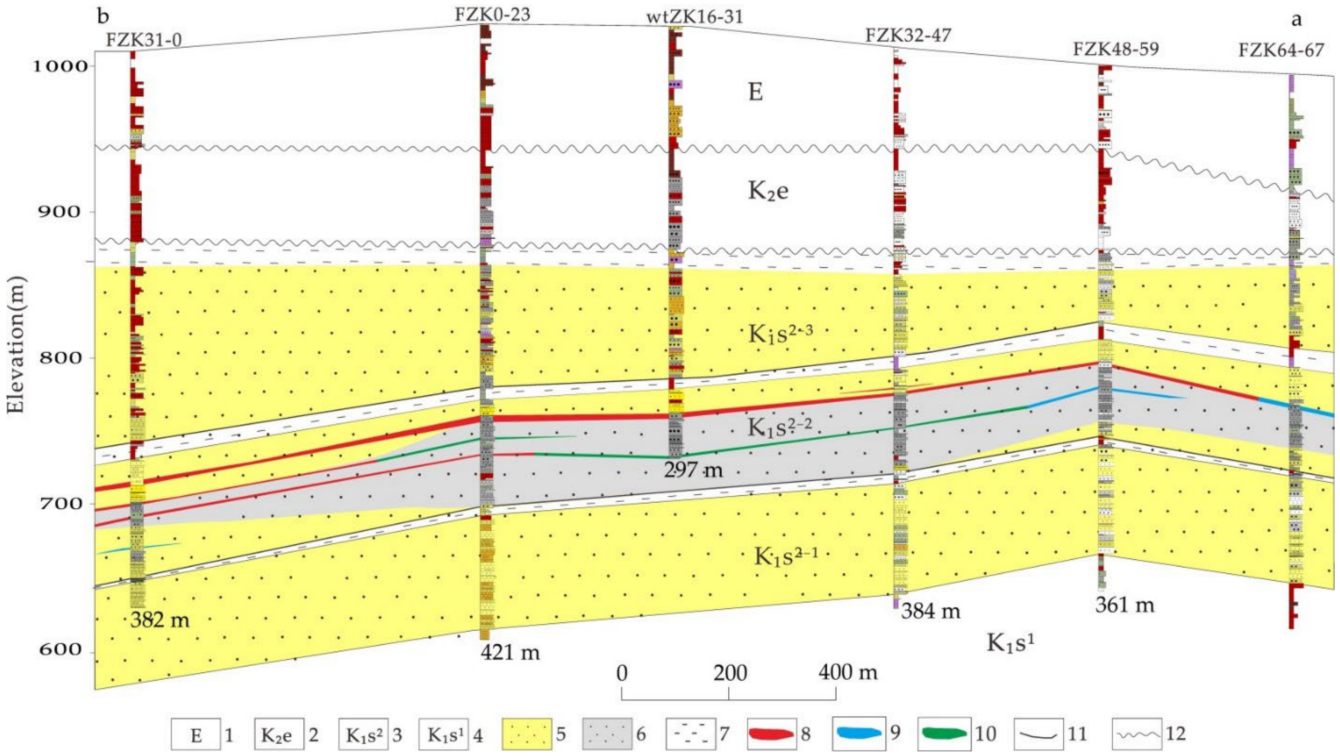


Figure 10. Geological profile of a–b in the Hadatu uranium deposits. 1—Paleogene strata. 2—Erlian group. 3—Upper part of Saihan group. 4—Bottom part of Saihan group. 5—Yellow oxidized sands. 6—Gray reducing sands. 7—Mudstone. 8—Uranium ore bodies. 9—Uranium mineralization. 10—Uranium abnormal. 11—Lithologic boundary. 12—Non-conformity boundary.

4.3.2. Three-Dimensional Seismic Exploration Results and Their Relationship with Mineralization Environment

The administrator has forbidden geological survey and research units from exploring the main northern mines, due to the enforcement of environmental protections in recent years. Therefore, a 3D high-resolution seismic prospecting experiment was performed in the southern sub-mining area, with a full fold area of 5 km^2, aiming at finely imaging the underground geological structures and understanding the metallogenic pattern that as yet remains unclear. The 3D data acquisition parameters are shown in Table 2 (HEXIN stage).

The typical inversion profile extracted from the 3D dataset, ranging from K_2e to K_1s^1, is shown in Figure 11. The *p*-wave impedance (a) and density (b) were calculated by pre-stack inversion; the resistivity (c) was inverted from the post-stack logging inversion based on seismic constraints, and the (d) lithology was calculated from the resistivity. In this picture, the inserted black lines show the gamma logging curve, and we know that most of the gamma data are located in the area with high resistivity, high impedance, and high density, as well as in the sand bodies.

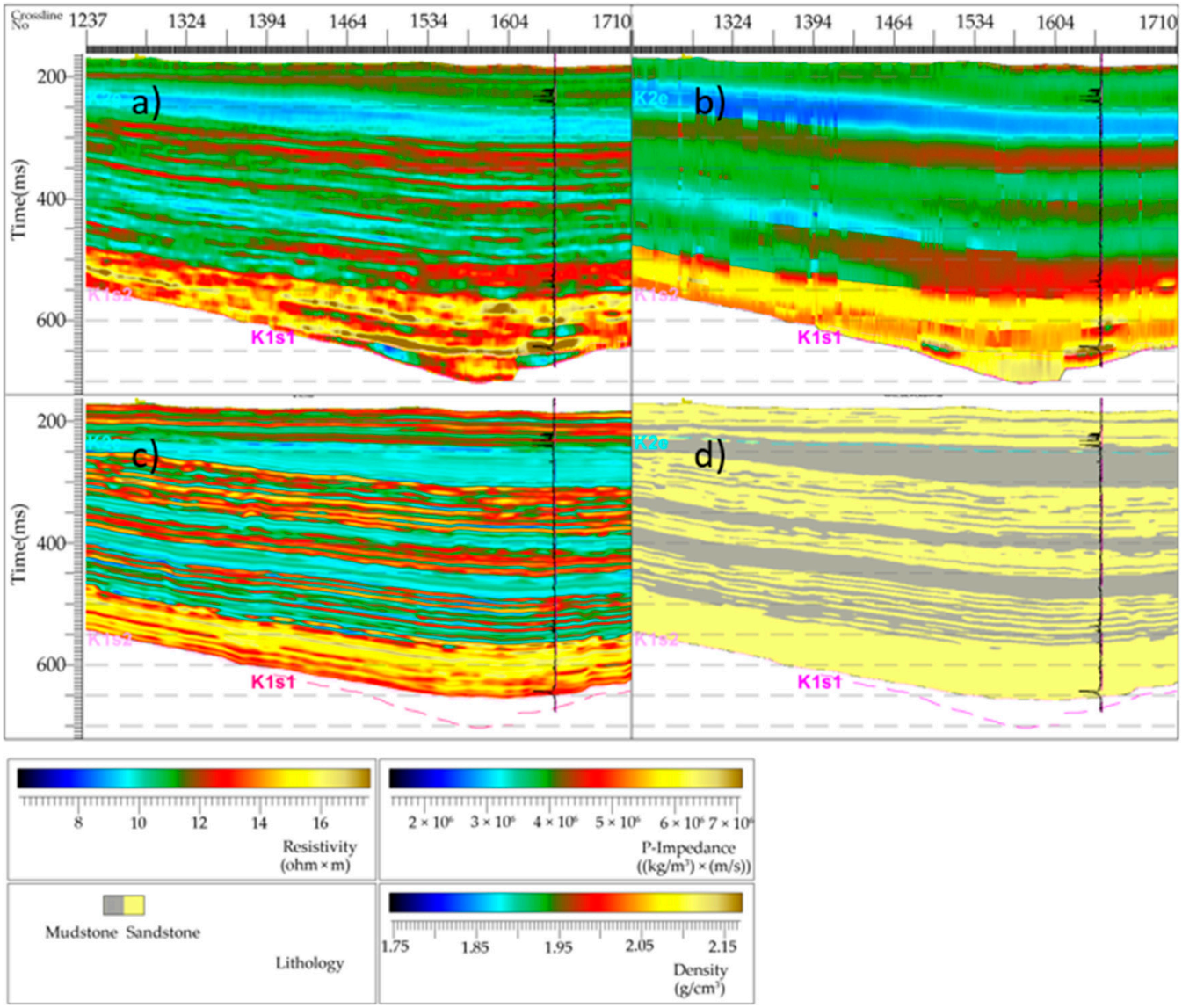


Figure 11. Inversion results of a typical cross-well line; *p*-wave impedance of target layer calculated by post-stack inversion (**a**), density of target layer calculated by pre-stack inversion (**b**), resistivity of target layer calculated by well loggings inversion method based on the constraint of seismic data (**c**), and lithology transformed by resistivity (**d**); the inserted curves of the four pictures are the gamma logging of the FZK497-255-t3 with U mineralization, ranging from 0 to 800 API.

The interpretation of the 3D stratigraphic morphology of K_1s in the time domain is given in Figure 12. There are four drilling holes in the research area, with confirmed industrial uranium mineralization of FZK497-255-t3 and EZK640-2099-t4, low-level uranium mineralization of EZK640-2067-t3, and non-abnormal mineralization of EZK640-2107-t2. The values of the gamma logging data from the boreholes are represented in the circles' sizes; the bigger the circles, the higher the gamma value. Furthermore, red and yellow also represent high gamma values, and blue and green represent low.

According to the inversion results and the 3D imaging of the target formation, the regions most favorable to U mineralization (e.g., FZK495-255-t3 and EZK640-2099-t4) have roughly three significant features: (1) A U-shaped "big depression" under the target formation (the upper section of K_1s), which has a thick, reducing strata (e.g., K_1t FM and K_1a FM in the Erlian basin); this feature also arises in the two deposits mentioned above. (2) There are faults or fractures that could connect the target formation to the deep

reducing formation. (3) Ore-containing strata are located near sand bodies and are basically characterized by high impedance, density, and resistivity—properties that can be obtained by seismic inversion.

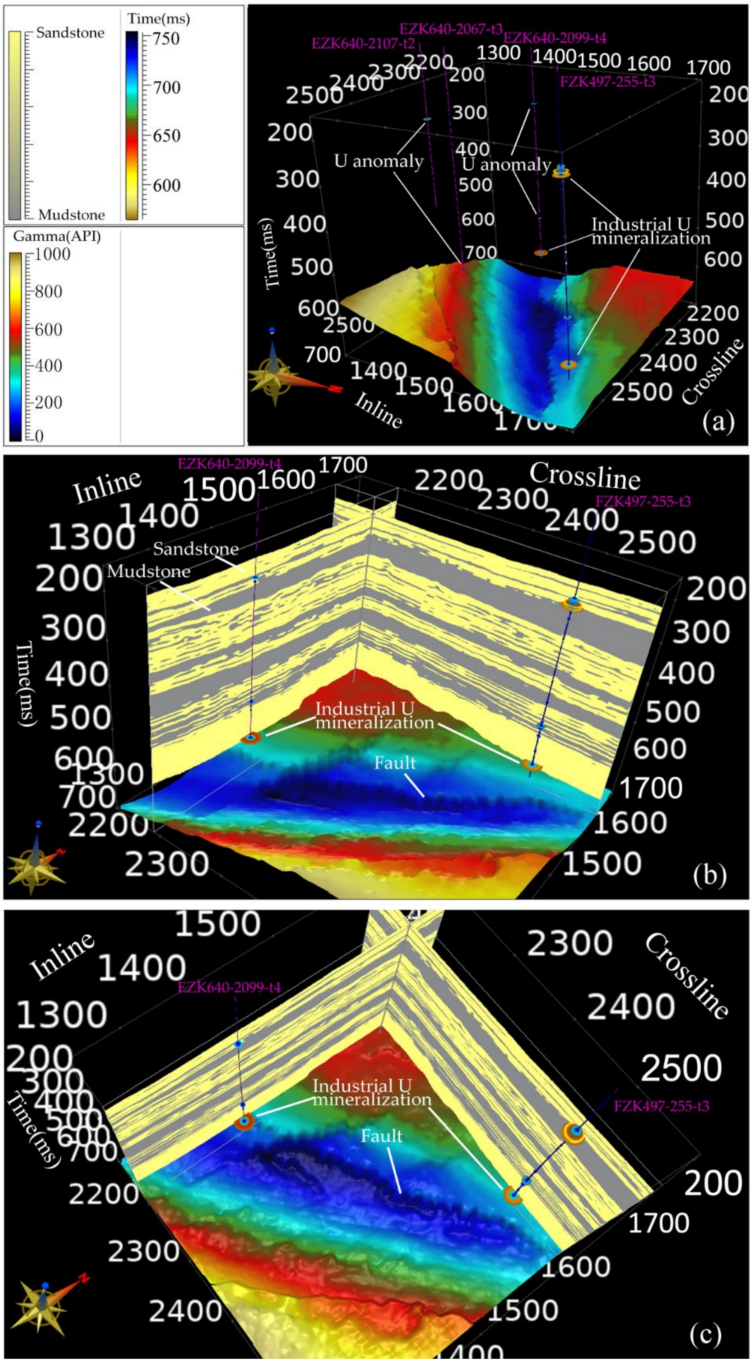


Figure 12. Three-dimensional distribution of the K_1s bottom boundary and gamma logging (**a**), lateral view of K_1s bottom boundary and the rock lithological profiles of the upper part of the K_1s FM (**b**), top view of 3D distribution map (**c**); the yellow represents sandstone and the gray represents mudstone in the two cross profiles. Red and yellow circles represent high gamma values, and blue circles represent low gamma values; in the 3D surface map, the yellow represents shallow burial depth and the blue means great depth; the two industrial U mineralization boreholes, FZK495-255-t3 and FZK495-2099-t4, located in the fracture and depression sections; the U abnormal hole of EZK640-2067-t3, and the normal borehole of EZK640-2107-t2 are located where there are no fractures or depression characteristics.

It is worth mentioning that no industrial U mineralization has been found in the positions of EZK640-2067-t3 and EZK640-2107-t2, although there is a U-shaped "big depression" under the target layer, and there are sand bodies in the target formation. Figure 10 shows that there are no faults that connect the deep and shallow formations under the area in which two boreholes appear, and faults may strongly determine uranium mineralization. In Figure 13, there are two layers of U mineralization in FZK495-255-t3 and EZK640-2099-t4; the shallow ones are medium-grade uranium mineralizations with an average gamma value of about 250 API at 530 ms and 500 ms, respectively, and the deep ones have the highest gamma values of about 1271 and 2467 API, respectively, which are far beyond the standard industrial grades of 680 ms in the FZK495-255-t3 and 600 ms in the EZK640-2099-t4.

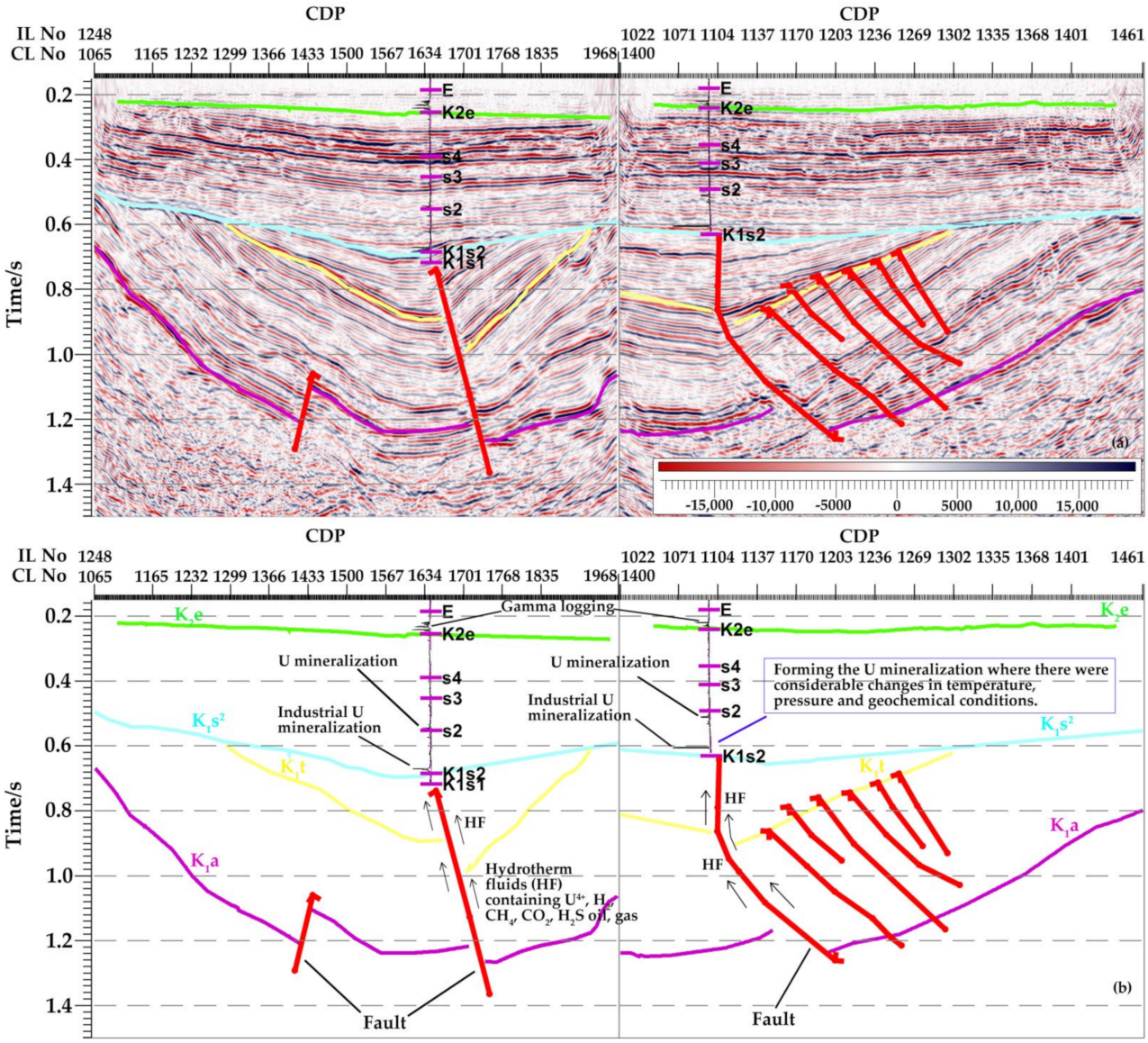


Figure 13. The interpretation of the cross-well seismic profile (**a**) and the prediction of the U-forming process (**b**).

Additionally, the logging data of the Hadatu deposits show that the deepest industrial uranium mineralization is about 650 m down (shown in Figure 3). It was very difficult to mineralize at such depths in previous SUDs studies; the phenomenon whereby high-grade U mineralization occurs at great depth cannot be easily clarified by traditional roll-front metallogenic mechanisms in the Erlian basin. In order to explain this occurrence, we

here propose the hypothesis of "hydrothermal effusion" mineralization over conventional mineralization, mainly inspired by seismic interpretation; meanwhile, some mineralogical evidence suggests the participation of hydrothermal fluids [49]. As such, we assume the mineralization process may occur as follows (shown in Figure 13): thick reducing strata were deposited in the K_1t and K_1a periods, and U preconcentration occurred in the reducing formation. The target sandstone was deposited in the Cretaceous Saihan period. Afterwards, as a result of Earth's dynamics, an upward migration of hydrothermal fluids occurred, as the hydrothermal fluids originating from the reducing formation (K_1t and K_1a) migrated upward along the faults or fraction zone into the shallow target sand. In the preprocess, the fluids carried a certain amount of U^{4+}, H_2, CO_2, and other reducing materials (e.g., oil, gas, CH_4, H_2S). When the hydrothermal fluids flowed through the reducing formations, they carried some reductive materials out with them; this led to the further enrichment of the reducing agent in the fluids. Consequently, U-bearing and highly reductive fluids moved into the shallow target sandstone, and then physicochemical reactions took place. Physically, the uranium in the fluids may have been liberated due to the drop in temperature and pressure; chemically, the U may have been precipitated owing to a redox reaction occurring when the fluids encountered the oxidized sand of the target formation. At the time the SUD formed, the grade of the ore deposits would have been high, given the superposition of the newly formed U mineralization and the pre-enriched U.

Furthermore, the deep, high-pressure hydrothermal fluids moved into weak sandstone and areas with high porosity, and depressurization belts could easily have formed layered alteration zones, which is why Hadatu ore bodies are usually tabular in shape. It is worth mentioning that multi-layer U mineralization may occur via "hydrothermal effusion" because multi-layer excretion channels can exist for as long as the conditions are appropriate. However, the mineralization grade declined gradually from deep to more shallow layers, and we had already observed the phenomenon at 550~680 ms in FZK495-255-t3 and at 500~600 ms in EZK640-2099-t4.

4.4. Prediction Pattern

Although geophysical seismic methods cannot provide direct evidence of uranium mineralization like mineralogy and geochemistry data can, seismic exploration results can offer substantial information useful in understanding the lateral property changes in geological bodies and inferring the indirect features (e.g., formations, faults, and sand bodies) of the research area, including places with mines or without mines. As such, using the seismic study results, a contrast analysis of the mineralization environment can be performed easily on a given region, which is impossible in ore mineralogy studies and in other works on local regions.

The 2D and 3D seismic prospecting results can generally be used to reveal the target formation and its shape, faults, and their characteristics, and the distribution of target sandstone. By comparison, seismic imaging usually offers clearer geological information, derived from the exploration of the three important SUDs in the Erlian basin. Using our seismic interpretation, we have successfully predicted the most favorable U mineralization site, shown at 3200 CDP in Figure 6. Therefore, we propose two morphological prediction patterns (Figure 14).

(1) The Bayanwula pattern: (a) The morphology of the target formation is characterized by a "U" shape, and the most favorable U mineralization site would be found in the sloping zones on either side of the "U", as slopes are conducive to the flow of underground fluid. (b) "Big depression" reducing formations are another area that is advantaged in terms of U mineralization; they could provide sufficient reductive material for the redox reaction to promote U mineralization. (c) Interpreted Cretaceous faults extending from deep strata to shallow strata are key factors, because they may become channels enabling the raising of hydrothermal fluids and reducing mediums from the depths. (d) Sand bodies in the target layer were present above the deep reducing formation, which is favorable as it means there are faults connecting the target sand bodies and the reductive formation, and the

target sandstone often has seismic facies with weak–medium amplitudes, low–medium frequencies, and low continuity.

(2) Hadatu (roughly including Saihangaobi) pattern: (a) The configuration of the target sandstone layer is also "U"-shaped, and the two sloping zones offer favorable U mineralization sites because they favor the flow of O-U-bearing groundwater. (b) There is a thick reducing deposition under the target layer. (c) There is a large-angle non-conformity (greater than 20 degrees) between the overlying target formation in shallow areas and the reducing formation at depth. (d) There are faults connecting the deep reducing formation and shallow sand bodies, and these faults are beneficial to the raising of deep hydrothermal fluids and reducing materials. (e) There are sand bodies in the target formation, and sandstone usually has seismic facies with weak–medium amplitudes, low–medium frequency, and low continuity.

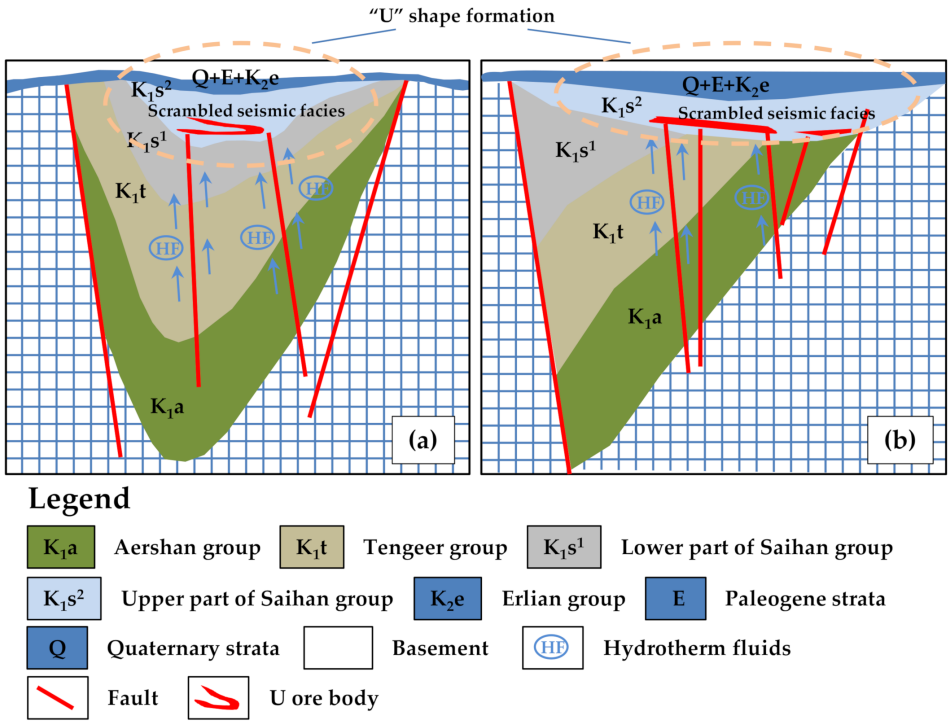


Figure 14. The prediction patterns of SUDs in the Erlian basin. (**a**) the Bayanwula pattern means "Big depression + fault", (**b**) the Hadatu pattern means "Large-angle non-conformity + fault".

Previous studies have shown that pyrite alterations exist in the U mineralized formation of the Hadatu deposits and other SUDs [49], and the pyrite mineralization is considered to have been caused by deep hydrothermal fluids, which raises a question: where did they come from? An idea referred to as "hydrothermal effusion" has been formed from the observations made in Figure 13, in which the deep hydrothermal fluids came from faults or non-conformities to target sand bodies, and pyrite mineralization may have been triggered by these fluids. On the other hand, the presence of pyrite mineralization also verifies the validity of the two prediction patterns mentioned above. In the future, studies may use seismic velocity and inverted density to reveal the pyrite alterations associated with SUDs.

A recent experiment showed that there are some petrophysical differences between U-bearing samples and uranium-free samples (shown in Figure 15) in the Hadatu deposit [62]. In the future, seismic attributes and inversion technologies may be used to directly predict the location of uranium mineralization. The aim of this work has been to determine the statistical petrophysical differences between the ore and the surrounding rocks in the SUD environment.

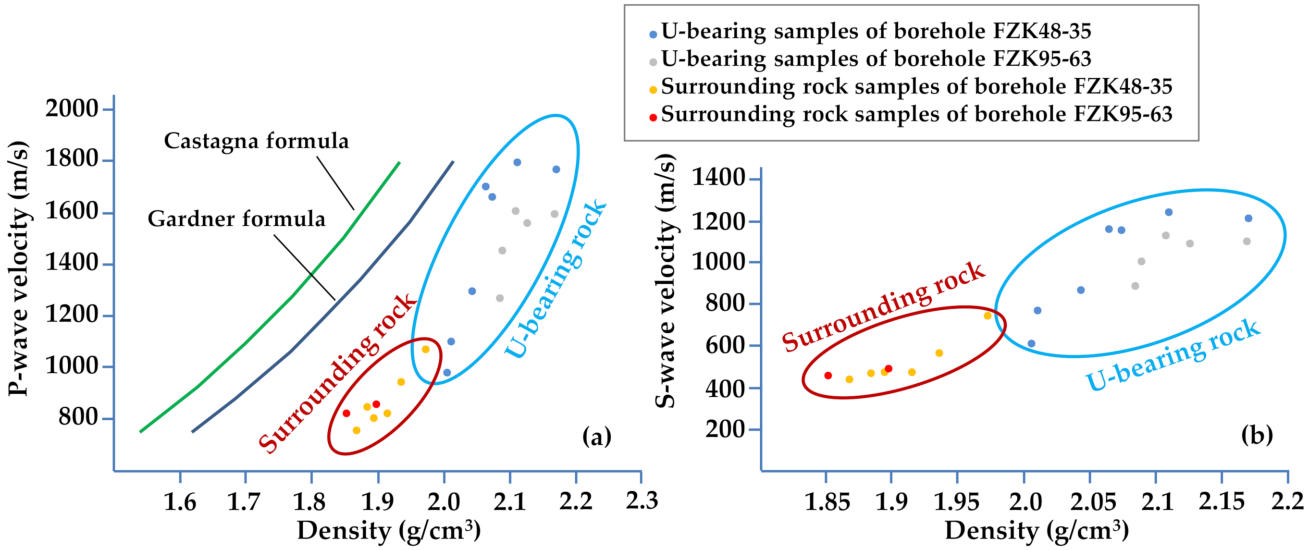


Figure 15. Experimental results of petrophysical parameters for uranium-bearing rock and the surrounding rock in the Hadatu deposits. (**a**) *p*-wave and density; (**b**) *s*-wave and density.

5. Conclusions

(1) Extensive explorations and the practicing of geophysical methods suggest that the significant ore-controlling factors could be identified by 2D or 3D seismic prospecting. In particular, 3D seismic imaging could provide precise information about "'U'-shaped layers", "big depressions of reducing formation", "large-angle non-conformities", "faults with long-term activity, and "sandstone and its seismic facies", resulting in accurate predictions of areas favoring U mineralization in subsequent drilling programs.

(2) Some suggestions for SUD seismic exploration are made, as follows: firstly, the number of acquisition folds needs to be more than 40 when undertaking shallow imaging, and broadband excitation and receiving are required to improve the resolution of the following inversion. Secondly, the processing steps of denoising and deconvolution should be considered more closely. Thirdly, it is important to understand the stratum configuration and fault characteristics, and the sandstone in the target formation and its seismic facies should also be studied in greater detail.

(3) Two morphological prediction patterns of SUDs, named "Big depression + fault" and "Large-angle unconformity + fault", have been proposed based on high-resolution seismic studies, despite the fact that reliable seismic responses indicating SUDs have yet to be found so far. These patterns will provide an important scientific basis for future SUD seismic work.

(4) The understanding of the deep hydrothermal genesis of U mineralization in the Erlian basin is insufficient compared to the other SUDs in northern China, although some achievements have been made. Based on the information in picture 13, we propose "hydrothermal effusion" mineralization. This suggests for the first time that hydrothermal fluids are involved in U mineralization, and organic matter originating from reducing formations might promote redox U mineralization.

Author Contributions: Conceptualization, Q.W., Y.W. and Z.L. (Zying Li); Data curation, Q.W., X.Y., Z.L. (Ziwei Li) and Z.P.; Formal analysis, Q.W., B.Q., W.H. and C.C.; Investigation, Q.W., C.C., Z.L. (Ziwei Li) and Z.P.; Methodology, Q.W. and Y.W.; Project administration, Q.W. and Z.L. (Ziying Li); Supervision, Y.W. and Z.L. (Ziying Li); Visualization, Q.W. and Z.L. (Ziying Li); Writing—Original draft, Q.W.; Writing—Review and editing, X.Y., C.C., Z.L. (Ziwei Li), Z.P. and Y.H. All authors have read and agreed to the published version of the manuscript.

Funding: This research was funded by LONG CAN II Project and Key Technologies of Fourth-Generation Uranium Exploration from China National Nuclear Corporation (Grant No are 2018-111 and 2021-143, respectively).

Data Availability Statement: No new data were created in this study. Data sharing is not applicable to this article.

Acknowledgments: We are highly thankful to the Airborne Survey and Remote Sensing Center of CNNC for offering raw resources in the study areas. Many thanks are given to the editors and reviewers for precious comments.

Conflicts of Interest: The authors declare no conflict of interest.

References

1. Zhang, J.D.; Xu, G.Z.; Lin, J.R. The implication of six kinds of new sandstone-type uranium deposits touranium resources potential in North China. *Geol. China* **2010**, *37*, 1434–1450.
2. Bonnetti, C.; Cuney, M.; Michels, R.; Truche, L.; Malartre, F.; Liu, X.D.; Yang, J.X. The Multiple Roles of Sulfate-Reducing Bacteria and Fe-Ti Oxides in the Genesis of the Bayinwula Roll Front-Type Uranium Deposit, Erlian Basin, NE China. *Soc. Econ. Geol.* **2015**, *110*, 1059–1081. [CrossRef]
3. Cheng, Y.H.; Wang, S.Y.; Jin, R.S.; Li, J.G.; Ao, C.; Teng, X.M. Global Miocene tectonics and regional sandstone-style uranium mineralization. *Ore Geol. Rev.* **2019**, *106*, 238–250. [CrossRef]
4. IAEA. *Uranium 2016: Resources, Production and Demand*; IAEA: Vienna, Austria, 2016.
5. IAEA. *IAEA Tecdoc Series: Geological Classification of Uranium Deposits and Description of Selected Examples*; IAEA: Vienna, Austria, 2018.
6. Chen, F.X.; Nie, F.J.; Zhang, C.Y.; Zhang, Z.F. Geological characteristics and genetic mechanism of the Honghaigou uranium deposit in the Southern Margin of Yili Basin. *Acta Geol. Sin.* **2016**, *90*, 3324–3336.
7. Wang, G.; Chen, Z.L.; Wang, G.R.; Lu, K.G.; Zhang, Z.F.; Kang, Y.; Jiang, H.; Ren, M.C.; Han, F.B.; Zhou, Z.J. Up-welling leakage-recharge genetic model of the Mengqiguer sandstone-type uranium deposit, southern Yili Basin, NW China. *Ore Geol. Rev.* **2021**, *138*, 104369. [CrossRef]
8. Ni, S.Q.; Song, J.Y.; Cai, Y.Q.; Zhang, X.; Li, Z.Z.; Qiu, Y.B.; Zhang, H.J.; Jiang, H. Sedimentary Characteristics and Evolution of the Middle Jurassic Xishanyao Formation in the Langka area, Southern Margin of the Yili Basin. *Acta Sedimentol. Sin.* **2021**, *39*, 434–445.
9. Zhang, L.; Liu, C.; Lei, K. Green altered sandstone related to hydrocarbon migration from the uranium deposits in the northern Ordos Basin, China. *Ore Geol. Rev.* **2019**, *109*, 482–493. [CrossRef]
10. Cai, C.F.; Li, H.T.; Qin, M.K.; Luo, X.R.; Wang, F.Y.; Ou, G.X. Biogenic and petroleum-related ore-forming processes in Dongsheng uranium deposit, NW China. *Ore Geol. Rev.* **2007**, *32*, 262–274. [CrossRef]
11. Chen, G.X.; Sun, Z.X.; Nie, F.J.; Li, C.L.; Zhen, Y.C.; Zhou, Z.K. Hydrogeochemical characteristics of the sandstone-hosted uranium mineralization in northern Ordos Basin, China. *Ore Geol. Rev.* **2020**, *126*, 103769. [CrossRef]
12. Yang, D.G.; Wu, J.H.; Nie, F.H.; Bonnetti, C.; Xia, F.; Yan, Z.B.; Cai, J.F.; Wang, C.D.; Wang, H.T. Petrogenetic Constraints of Early Cenozoic Mafic Rocks in the Southwest Songliao Basin, NE China: Implications for the Genesis of Sandstone-Hosted Qianjiadian Uranium Deposits. *Minerals* **2020**, *10*, 1014. [CrossRef]
13. Li, Y.; Nie, F.J.; Jia, L.C.; Lu, S.J.; Yan, Z.B. Geochemical Characteristics, Palaeoenvironment and Provenance of Uranium-Bearing Sandstone in the Sifangtai Formation, Northern Songliao Basin, Northeast China. *Minerals* **2021**, *11*, 1019. [CrossRef]
14. Bonnetti, C.; Cuney, M.; Bourlange, S.; Deloule, E.; Poujol, M. Primary uranium sources for sedimentary-hosted uranium deposits in NE China: Insight from basement igneous rocks of the Erlian Basin. *Miner. Depos.* **2016**, *52*, 297–315. [CrossRef]
15. Zhang, B.; Wang, X.; Zhou, J.; Han, Z.; Liu, W.; Liu, Q.; Wang, W.; Li, R.; Zhang, B.; Dou, B. Regional geochemical survey of concealed sandstone-type uranium deposits using fine-grained soil and groundwater in the Erlian basin, north-east China. *J. Geochem. Explor.* **2020**, *216*, 106573. [CrossRef]
16. Nie, F.J.; Yan, Z.B.; Feng, Z.B.; Li, M.G.; Xia, F.; Zhang, C.Y.; Wang, Y.G.; Yang, J.X.; Kang, S.H.; Shen, K.F. Genetic models and exploration implication of the paleochannel sandstone-type uranium deposits in the Erlian Basin, North China—A review and comparative study. *Ore Geol. Rev.* **2020**, *127*, 103821. [CrossRef]
17. Cai, Y.Q.; Zhang, J.D.; Li, Z.Y. Outline of Uranium Resources Characteristics and Metallogenetic Regularity in China. *Acta Geol. Sin.* **2015**, *89*, 1051–1069.
18. Nie, F.J.; Li, M.G.; Yan, Z.B.; Xia, F.; Zhang, C.Y.; Yang, J.X.; Kang, S.H.; Shen, K.F. Segmentation of the target layer Saihan Formation and sandstone-type uranium mineralization in Erlian Basin. *Geol. Bull. China* **2015**, *10*, 952–963.
19. Li, W.T.; Li, Z.Y.; Kang, S.H.; Li, X.D.; Liu, W.S. Study on uranium occurrences in Hadatu uranium deposit, Erlian Basin. *Geol. Rev.* **2019**, *A1*, 157–158.
20. Liu, W.S.; Zhao, X.Q.; Kang, S.H.; Shi, Q.P.; Zhang, Z.N. Inversion structure and its relationship with sandstone type uranium metallization in Erlian Basin. *Uranium Geol.* **2018**, *34*, 81–89.

21. Lu, C.; Jiao, Y.Q.; Peng, Y.B.; Yang, J.X.; Chen, F.Z. Effect of the episodic rifting in the western manite depression in Erlian Basin on sandstone-type uranium mineralization. *Acta Geol. Sin.* **2016**, *90*, 3483–3491.
22. Liu, W.S.; Li, X.D.; Xue, Z.G.; Liu, Y.H.; Liu, C.H. Geochemical characteristics and geological significance of Hadatu uranium deposit in Erlian Basin, Inner Mongolian. *Uranium Geol.* **2020**, *36*, 325–336.
23. Yan, Y.; Zhang, Z.S.; Shi, Q.P. Trace element geochemical characteristics of Bayanwula uranium deposit in Erlian basin. *World Nucl. Geosci.* **2019**, *36*, 21–29.
24. Kang, H.; Chen, Y.L.; Li, D.P.; Zhao, J.X.; Cui, F.R.; Xu, Y.L. Deep-penetrating geochemistry for concealed sandstone-type uranium deposits: A case study of Hadatu uranium deposit in the Erenhot Basin, North China. *J. Geochem. Explor.* **2020**, *211*, 106464. [CrossRef]
25. Lu, M.; Ye, R.; Zhang, B.M. Source identification of the geochemical anomaly from the fine-grained soil survey in the Nuheting sandstone-type uranium deposit, Erlian Basin, north China. *J. Geochem. Explor.* **2021**, *227*, 106797. [CrossRef]
26. Ke, D.; Liu, H.J.; Hou, H.Q.; Wu, G.D.; Hao, W.J. Formation mechanism of electro-geochemical anomalies in interlayered oxidation type sandstone-hosted uranium deposit and its prospecting significance. *Acta Geol. Sin.* **2016**, *90*, 3545–3553.
27. Liu, X.Y.; Li, B. Current status of in-situ leachable sandstone-type uranium drilling and technical measures of improving drilling efficiency. *Drill. Eng.* **2021**, *48*, 35–41.
28. Chen, X.G.; Xiang, P. Application of gravity, magnetic, electric and seismic comprehensive geologic modeling method for piedmont zone of Hala'alate mountain in Junggar Basin. *J. China Univ. Pet. (Ed. Nat. Sci.)* **2017**, *41*, 65–74.
29. Mehrdad, D.; Colin, G.F.; Peter, G.L. Clustering and constrained inversion of seismic refraction and gravity data for overburden stripping: Application to uranium exploration in the Athabasca Basin, Canada. *Geophysics* **2020**, *85*, 133–146.
30. Chen, C.; Yu, X.; Chen, T. Study on the mechanism of magnetic anomaly in the redox transitional zone of Bayan Ula uranium deposit. *Geol. Rev.* **2017**, *63*, 55–56.
31. Zhang, S.B.; Tan, C.L.; Jiang, Y.Y.; Wu, D.Y. Pre-selection tests on geophysical and geochemical exploration methods for in-situ leachable sandstone-type uranium deposit in Erlian Basin. *Uranium-Geol.* **1997**, *13*, 109–116.
32. Yu, X.; Li, X.D.; Wan, H.P.; Hu, Y.C. Research and application of AMT method in the south of tengger depression Erlian basin. *J. East China Inst. Technol. (Nat. Sci. Ed.)* **2017**, *40*, 362–367.
33. Wang, H.F.; Liu, B.; Chen, S.; Chen, F.X.; Xue, W.H. Application of integrated geophysical survey to sedimentary rock type uranium exploration in the Erlian Basin. *Geol. Explor.* **2019**, *55*, 127–134.
34. Dentith, M.; Randell, M. Sandstone-type uranium deposits in South Australia and North America: A comparison of their geophysical characteristics. ASEG Extended Abstracts. In Proceedings of the 16th Geophysical Conference & Exhibition, Adelaide, SA, Australia, 16–19 February 2003; Australian Society of Exploration Geophysicists: St. Leonards, NSW, Australia, 2003; pp. 233–248.
35. Wu, Q.B.; Cao, C.Y.; Pan, Z.Q.; Li, Z.W.; Qiao, B.P. An analysis of test result of the hammering small-refraction method used in near-surface survey. *Geophys. Geochem. Explor.* **2016**, *40*, 380–384.
36. Wu, Q.B.; Li, Z.W.; Pan, Z.Q.; Cao, C.Y.; Qiao, B.P. Study on some problems in the seismic exploration of sandstone type uranium deposits. *Prog. Geophys.* **2017**, *32*, 2097–2106.
37. Wu, Q.B.; Liu, W.S.; Li, Z.W.; Pan, Z.Q.; Cheng, J.X. The test of seismic technology for locating the paleo-valley. *Uranium Geol.* **2015**, *31*, 193–198.
38. Wu, Q.B.; Huang, W.C.; Qiao, B.P. Integrated seismic prediction techniques research on sandstone-type uranium deposit:a case study of uranium deposit in Qiharigetu depression. *Prog. Geophys.* **2018**, *33*, 2002–2014.
39. Wu, Q.B.; Li, Z.W.; Pan, Z.Q. Application research on seismic detect technics for sandstone-type uranium deposits in the north of Ordos Basin. *Uranium Geol.* **2016**, *32*, 104–110.
40. Gyorfi, I.; Hajnal, Z.; White, D.J. High-resolution seismic survey from the McArthur River region: Contributions to mapping of the complex P2 uranium ore zone, Athabasca Basin, Saskatchewan. *Geol. Surv. Can.* **2007**, *588*, 397–412.
41. Manzi, M.S.D.; Gibson, M.A.S.; Hein, K.A.A..; King, N.; Durrheim, R.J. Application of 3D seismic techniques to evaluate ore resources in the West Wits Line goldfield and portions of the West Rand goldfield, South Africa. *Geophysics* **2012**, *77*, 163–171. [CrossRef]
42. Juhojuntti, N.; Wood, G.; Juhlin, C. 3D seismic survey at the Millennium uranium deposit, Saskatchewan, Canada: Mapping depth to basement and imaging post-Athabasca structure near the orebody. *Geophysics* **2012**, *77*, 245–258. [CrossRef]
43. Hajnal, Z.; Tak´acs, E.; Annesley, I.R.; Pandit, B. Effective utilization of seismic reflection technique with moderate cost in uranium exploration. *Geophys. Prospect.* **2020**, *68*, 129–144. [CrossRef]
44. Sun, Z.; Liu, Y.; Han, F.; Zhang, F.; Ou, X.; Cao, M.; Lei, A.; Yang, S.; Liu, M.; Gao, Z. Study on the 3D Sedimentary Characteristics of Sandstone Type Uranium Reservoir Based on 3D Seismic Attribute. *Minerals* **2021**, *11*, 1096. [CrossRef]
45. Wang, L.M.; Xu, G.C. *Shallow Seismic Exploration Report in Mandepression Yi and Kohler-Dai Lama Temple in Erlian Basin, Inner Mongolia*; Nuclear Industry Navigation Survey and Remote Sensing Center: Shijiazhuang, China, 2004.
46. Wu, Q.B.; Qiao, B.P.; Huang, W.C. *Development and Application of 3D Seismic Exploration Technology for Sandstone Type Uranium Deposits*; Beijing Research Institute of Uranium Geology: Beijing, China, 2017.
47. Wu, Q.B.; Wang, S.; Yang, L.Q.; Yang, H.J.; Wang, Y.; Huang, W.C. *Study on Comprehensive Interpretation of Sandstone Uranium Mineral Exploration Data in Erlian Base*; Beijing Research Institute of Uranium Geology: Beijing, China, 2021.

48. Nie, F.J.; Li, M.G.; Deng, J.Z.; Yan, Z.B.; Zhang, C.Y.; Jiang, M.Z.; Yang, J.X.; Kuang, W.Z.; Kang, S.H.; Shen, K.F. Multiple type uranium deposit assemblage and uranium exploration in Erlian rift Basin, Inner Mongolia. *Miner. Depos.* **2015**, *34*, 711–729.
49. Qiu, L.F.; Li, X.D.; Liu, W.S.; Hu, B.Q.; Gao, L.; He, Z.B. Uranium Deposits of Erlian Basin(China): Role of Carbonaceous Debris Organic Matter and Hydrocarbon Fluids on Uranium Mineralization. *Minerals* **2021**, *11*, 532. [CrossRef]
50. Liu, B.; Miao, A.S.; Peng, Y.B.; Zhang, P.F.; Li, P.; Shen, K.F.; Shi, Z.Q. Research advances in uranium metallogenic characteristics, mechanism and dynamic background in the Mesozoic-Cenozoic basins of the Xingmeng area, North China. *Acta Geol. Sin.* **2020**, *94*, 3689–3711.
51. Bonnetti, C.; Malartre, F.; Huault, V.; Cuney, M.; Bourlange, S.; Liu, X.D.; Peng, Y.B. Sedimentology, stratigraphy and palynological occurrences of the late Cretaceous Erlian Formation, Erlian Basin, Inner Mongolia, People's Republic of China. *Cretac. Res.* **2014**, *48*, 177–192. [CrossRef]
52. Dahlkamp, F.J. *Uranium Deposits of the World*; Springer: Berlin, Germany, 2016; ISBN 978-3-540-78553-8.
53. Nie, F.J.; Li, M.G.; Yan, Z.B. Lateral oxidation mineralisation in palaeo-channel, sandstone-type uranium deposit—A case study from Bayanwula Area, Erlian Basin, Inner Mongolia, China. *AusIMM Bull. J. Australas. Inst. Min. Metall.* **2013**, *6*, 32–37.
54. Wu, Q.B.; Chen, C.; Yang, L.Q.; Yu, X.; Gao, L.J.; Zhou, J.J.; Li, B.H.; Wang, S.; Liu, W.S. Study of integrated geophysical characteristics of paleo-valley sandstone-type uranium deposits in the middle of the Erenhot basin. *Acta Geol. Sin.* **2021**, *95*, 2521–2536.
55. Wu, Q.B.; Li, Z.W.; Pan, Z.Q. Application status and future trend of seismic exploration techniques in sandstone uranium deposits. *Geophys. Geochem. Explor.* **2017**, *41*, 648–655.
56. Wu, Q.B.; Huang, Y.C. Indications of sandstone-type uranium mineralization from 3D seismic data: A case study of the Qiharigetu deposit, Erenhot Basin, China. *J. Pet. Explor. Prod.* **2021**, *11*, 1069–1080. [CrossRef]
57. Harshman, E.N.; Adams, S.S. *Geology and Recognition Criteria for Roll-Type Uranium Deposits in Continent Sandstone*; US DOE GJBX-1(81); Adams (Samuel S.) and Associates: Boulder, CO, USA, 1981; p. 185.
58. Yan, Z.B.; Nie, F.J.; Hu, J.J.; Kang, S.H. Study on uranium occurrences of sandstone-type uranium deposit in Bayanwula area, Erlian basin, Inner Mongolia. In *Progress in Environmental Protection and Processing of Resource, Pts 1–4*; Trans. Tech. Publications Ltd.: Stafa-Zurich, Switzerland, 2013; Volumes 295–298, p. 2803.
59. Shor, G.M.; Markov, S.N.; Rubinov, I.M.; Peshkov, P.A. Paleochannel type uranium deposits in western Siberia and Transbaikal regions. *Uranium Geol.* **2002**, *18*, 65–88.
60. Fischer, R.P. Similarities, differences, and some genetic problems of the Wyoming and Colorado plateau types of uranium deposits in sandstone. *Econ. Geol.* **1970**, *65*, 778–784. [CrossRef]
61. Li, W.T.; Li, Z.Y.; Li, X.D.; Liu, W.S.; Kang, S.H.; Lv, Y.H. Study on uranium occurring state in Hadatu sandstone-type uranium deposit in Erlian basin. *Uranium Geol.* **2020**, *24*, 150–154.
62. Li, Z.W.; Wu, Q.B.; Cao, C.Y. Preliminary Study on the Difference of Impedance Between Ore-bearing Sandstone and Wall Rock in Sandstone-type Uranium deposit: A Case Study of Well Core Samples in Hadatu Deposit. *Uranium Geol.* **2020**, *36*, 424–431.